PUBLICATION

MUSTANG

A MUltiple Space and Time scale Approach for the quaNtification of deep saline formations for CO_2 storaGe

Project Number:227286

AUTHORS: *David Stevens, Henry Power*

TITLE: *A scalable meshless formulation based on RBF Hermitian interpolation for 3D nonlinear heat conduction problems*

The research leading to these results has received funding from the European Community's Seventh Framework Programme [FP7/2007/2013) under grant agreement n° [227286]

Status	AUTHOR VERSION
Date	2010
Publisher	Tech Science Press
Reference	Hydrology & Earth System Sciences, Vol. 13, p. 1399

A scalable meshless formulation based on RBF Hermitian interpolation for 3D nonlinear heat conduction problems

David Stevens, Henry Power

School of Mechanical, Materials and Manufacturing Engineering,
University of Nottingham, Nottingham, UK

* Correspondence Author: H. Power, henry.power@nottingham.ac.uk

January 27, 2010

Abstract

Problems involving nonlinear time-dependent heat conduction in materials which have temperature-dependent thermal properties are solved with a novel meshless numerical solution technique using multiquadric radial basis functions (RBFs). Unlike traditional RBF collocation methods, the local Hermitian interpolation (LHI) method examined here can be scaled to arbitrarily large problems without numerical ill-conditioning or computational cost issues, due to the presence of small overlapping interpolation systems which grow in number but not in size as the global dataset grows. The flexibility of the full-domain multiquadric collocation method to directly interpolate arbitrary boundary conditions is maintained, via the local interpolations.

The Kirchhoff transformation is employed to reduce the degree of nonlinearity in the governing PDE, and a high-resolution interpolation procedure is outlined to transform the various thermal properties to Kirchhoff-space. The implementation procedure is validated using a problem with analytical thermal properties and a known analytical solution. Additionally the procedure is validated against a problem with pointwise-measured material property data, and an analytical solution which is imposed via the body-source term. In this second case, the solution quality is compared with the traditional full-domain multiquadric collocation method.

1 Introduction

This paper considers heat transfer within materials which have temperature-dependent thermophysical properties (i.e. non-linear heat transfer). This type of problem has numerous applications within many different branches of science and engineering, such as; electrical conductors, solar systems, heat exchangers, phase change problems, and many others. For certain substances, the phase change occurs over a relatively wide range of temperatures, with a relatively smooth variation of the thermophysical properties with temperature as the phase changes. In this case, their numerical solutions can be easily obtained with standard numerical approaches. However, in many other materials the phase

change takes places with very little variation of temperature, and the heat capacity exhibits a strong (non-linear) dependence on temperature in this region. In this latter case, numerical difficulties are encountered when solving this type of problem using standard numerical techniques.

One of the most important characteristics of supercritical fluids is that their thermophysical properties exhibit strong (non-linear) dependence on the temperature, especially near the pseudocritical point; the temperature at which the specific heat reaches a peak for a given pressure (for more details see [1] and [2]). An interesting example of the type of non-linear heat transfer considered in this work is the possibility of modelling phase change, as can occur during the flow of supercritical CO2. Since there is no theory available for general non-linear partial differential equations, the analysis of strongly non-linear heat transfer problems, such as those mentioned above, becomes difficult, and robust numerical techniques are required. In this work a novel meshless numerical technique is presented, based on the use of multiquadric radial basic functions (RBFs) for the solution of strongly non-linear heat transfer problems.

Radial Basis Functions have traditionally been used to provide a continuous interpolation of scattered data sets. However, this interpolation also allows for the reconstruction of partial derivatives throughout the solution field, which can then be used to drive the solution of a partial differential equation. Since the interpolation takes place on a scattered dataset with no local connectivity, the solution is essentially meshless. RBF-based methods have been successfully used to solve a wide variety of PDEs in this fashion.

Such full-domain RBF methods are highly flexible and can exhibit spectral convergence rates [3]. However, in their traditional implementation (as described in section 2) the fully-populated matrix systems which are produced lead to computational complexities of at least order-N^2 with datasets of size N. In addition, they suffer from increasingly poor numerical conditioning as the size of the dataset grows, and also with increasingly flat interpolating functions. This is a consequence of ill-conditioning in the determination of RBF weighting coefficients (as demonstrated in [4]), and is described by Robert Schaback [5] as the uncertainty relation; better conditioning is associated with worse accuracy, and worse conditioning is associated with improved accuracy. Many techniques have been developed to reduce the effect of the uncertainty relation in the traditional RBF formulation, such as RBF-specific preconditioners [6, 7, 8, 9], or adaptive selection of data centres [10, 11]. However, at present the only reliable methods of controlling numerical ill-conditioning and computational cost as problem size increases are domain decomposition [12, 13, 14, 15], or the use of locally supported basis functions [16, 17, 18, 19].

Locally supported basis functions offer a straightforward approach to achieving order-N computational complexity, however multilevel solution techniques are required in order to achieve convergence in this case [18, 19]. Such multilevel methods require hierarchical datasets to be maintained, which can be a non-trivial task, particularly when dealing with scattered data. Alternatively, by taking the domain decomposition principle and applying it to very small and heavily overlapping local systems, a local RBF collocation method can be formulated. Since the individual RBF systems never grow too large, such methods can be scaled to arbitrarily large data-sets without numerical conditioning issues, and with order-N computational complexity. In recent years several such local RBF collocation techniques have been proposed, and applied a variety of problems (for example; [20, 21, 22, 23]). For a more comprehensive review of such methods see [24].

The method implemented in this work is known as the Local Hermitian Interpolation (LHI) method. Unlike most local RBF collocation methods it utilises the Hermitian RBF collocation formulation (see

section 2 for more details), and allows both the PDE-boundary and PDE-governing operators to be included directly in the local interpolation. The inclusion of the governing PDE in the basis functions is shown in [24] to significantly improve the accuracy and stability of solutions obtained for linear transport problems. Additionally, the incorporation of information about the convective velocity field into the basis functions was shown to have a stabilising effect, similar to traditional upwinding methods but without the requirement to alter the stencil configuration based on the local convective field. The LHI method has been successfully applied to a range of linear and nonlinear transport equations, both steady and transient, using a variety of explicit and implicit time advancement formulations (see [25, 26, 27]). Accurate solutions are obtained on a variety of structured and unstructured datasets in 3D.

The standard approach to the solution of linear and nonlinear heat conduction problems is the use of finite difference and finite volume methods with simple polynomial interpolants [28, 29, 30]. Due to the dominance of diffusion in most cases, central differencing techniques are commonly used to compute the heat fluxes. However, limiter methods (such as the unconditionally stable TVD schemes) may be used for nonlinear heat conduction problems where the effective convection term, which results from the non-zero variation of thermal conductivity with temperature, can be expected to approach the magnitude of the diffusive term (see, for example, [31]).

In [32] the full-domain Kansa's RBF collocation method (see section 2 for more details) is applied to a 2D heat transfer problem, using the approximated thermal properties of zirconium, tungsten and tantalum over a wide range of temperatures. The Kansa method is shown to work well with scattered datasets, and exhibits accuracy comparable to a finite difference approach. However, as with all full-domain RBF methods, the approach used will suffer severely from computational cost and numerical conditioning issues as the dataset size is increased.

In recent years there has been an increased interest in the implementation of various meshless methods to the numerical solution of direct and inverse heat transfer problems (for more detail see [33, 34, 35, 36, 37, 38]). The present work aims to introduce a localised RBF formulation which maintains the accuracy and the meshless flexibility of the method presented in [32], while being scalable to arbitrarily large 3D problems. The proposed implementation is validated using a hypothetical 3D problem with known material properties and a mixture of applied boundary conditions, using both steady-state and time-dependent formulations (see section 5). The problem examined in [32] is also replicated, to ensure that the solution accuracy is comparable to the full-domain Kansa's collocation method (section 7).

In addition, the present work utilises RBF collocation methods to allow a high-resolution transformation of pointwise material data to continuous functions in Kirchhoff-space, as an alternative to the piecewise linear approximations used in [32]. The interpolation procedure is validated using a hypothetical substance in which the material properties follow rapidly decaying curves. For more general scenarios, where the exact solutions are not known, an appropriate measure of transformation quality is suggested.

For a glossary of terms used to classify the various locations at which data is manipulated, see Table 1.

Test point:	Location about which a RBF is centred
Trial point:	Location at which a known constraint is applied
Data centre:	A location consisting of both a test and a trial point
Solution centre:	A data centre at which the constraint is the value of the solution field
Boundary centre:	A data centre at which the constraint is the value of the PDE boundary operator (found on boundary surfaces only)
PDE centre:	A data centre at which the constraint is the value of the PDE governing operator
Stencil:	A collection of data centres over which a RBF interpolation can be performed
Local system:	A RBF interpolation performed using a particular stencil
Local system centrepoint:	The location around which a local system is formed (always a location where a solution centre is present)

Table 1: List of terms describing locations at which data is manipulated

2 Basic RBF formulation

A radial basis function depends upon the separation distances of a set of functional centres, also known as trial points, and exhibits spherical symmetry around these centres. There are several commonly used radial basis functions (see [39]), however in this work the popular multiquadric RBF (equation (1)) will be used throughout, with $m = 1$.

$$\Psi(r) = \left(r^2 + c^2\right)^{\frac{m}{2}} \quad m \in 2\mathbb{Z}^+ - 1 \tag{1}$$

The multiquadric RBF is a conditionally positive definite function of order m, which requires the addition of a polynomial term of order $m-1$, together with a homogeneous constraint condition, in order to obtain an invertible interpolation matrix. The 'c' term is known as a 'shape parameter', and describes the relative width of the RBF functions about their centres. In practice, tuning of this parameter can dramatically affect the quality of the solution obtained. Increasing the value of c will lead to a flatter RBF. This will, in general, improve the rate of convergence at the expense of increased numerical ill-conditioning of the resulting linear system [40].

The use of radial basis functions (RBFs) as a method of scattered data interpolation was first introduced by Hardy [41]. Using a series of M functional centres, ξ_j, known as 'trial points', an RBF approximation to a function $f(x)$ can be formed via

$$f(x) \approx \sum_{j=1}^{M} \lambda_j \Psi\left(\|x - \xi_j\|\right) + \sum_{j=1}^{NP} \lambda_{j+M} P_{m-1}^{j}(x) \quad x \in \mathbb{R}^n \tag{2}$$

where P_{m-1}^{j} is the j^{th} term of an order $(m-1)$ polynomial, under the constraint

$$\sum_{j=1}^{NP} \lambda_j P_{m-1}^{k}(x_j) = 0 \quad k = 1, \ldots, NP \tag{3}$$

with NP being the total number of terms in the polynomial (determined by the polynomial order and the number of spatial dimensions). If the value of the function is known at N locations $\{x_i,\, f(x_i)\,,\ \ i = 1, ..., N\}$, known as test points, then suitable values of λ_j can be found, provided that $N \geq M$, via the solution of a linear system

$$\begin{bmatrix} \Psi(\|x_i - \xi_j\|) & P_m(x_i) \\ P_m^T(\xi_j) & 0 \end{bmatrix} \lambda_j = \begin{bmatrix} f(x_i) \\ 0 \end{bmatrix} \tag{4}$$

In most cases the set of trial points ξ_j is chosen to be the same as the set of test points x_i, leading to a fully-determined linear system. This data-interpolation formulation is to be used later (see section 6), to construct continuous functions for material properties from pointwise experimental data.

The meshless RBF method for solving PDEs, as described by Kansa [42, 43], constructs the continuous solution $u(x)$ of the PDE in much the same way as for interpolation:

$$u(x) = \sum_{j=1}^{N} \lambda_j \Psi(\|x - \xi_j\|) + \sum_{j=1}^{NP} \lambda_{j+N} P_{m-1}^{j}(x) \quad x \in \mathbb{R}^n \tag{5}$$

Consider a typical linear boundary value problem

$$\begin{aligned} L[u] &= f(x) \quad \text{on } \Omega \\ B[u] &= g(x) \quad \text{on } \partial\Omega \end{aligned} \tag{6}$$

where the operators $L[]$ and $B[]$ are linear partial differential operators on the domain Ω and on the contour $\partial\Omega$, describing the governing equation and boundary conditions respectively. Collocating the system at N distinct test locations, x_j, coinciding with the trial points ξ_j, leads to a system of equations

$$\begin{bmatrix} B[\Psi] & B[P_{m-1}] \\ L[\Psi] & L[P_{m-1}] \\ P_{m-1} & 0 \end{bmatrix} \lambda = \begin{bmatrix} g \\ f \\ 0 \end{bmatrix} \tag{7}$$

which is fully populated and non-symmetric. This approach, known as Kansa's method, or the unsymmetric method, has been applied to a wide range of problems with great success (see for example [44, 45, 46, 47]). However, for the standard formulation there is no guarantee that the collocation matrix will be non-singular [11]. It can, in fact, be shown that for some data-centre distributions the collocation matrix will become singular [48].

An alternative approach proposed by Fasshauer [49] applies the boundary and PDE operators to the RBFs within the solution construction:

$$u(x) = \sum_{j=1}^{NB} \lambda_j B_\xi \Psi(\|x - \xi_j\|) + \sum_{j=NB+1}^{N} \lambda_j L_\xi \Psi(\|x - \xi_j\|) + \sum_{j=1}^{NP} \lambda_{j+N} P_{m-1}^{j}(x) \tag{8}$$

Collocating in a similar way leads to the system of equations

$$\begin{bmatrix} B_x B_\xi [\Psi] & B_x L_\xi [\Psi] & B_x [P_{m-1}] \\ L_x B_\xi [\Psi] & L_x L_\xi [\Psi] & L_x [P_{m-1}] \\ B_\xi [P_{m-1}]^T & L_\xi [P_{m-1}]^T & 0 \end{bmatrix} \lambda = \begin{bmatrix} g \\ f \\ 0 \end{bmatrix} \tag{9}$$

In the above matrix equation, the operators with ξ subscript are applied to the trial points and the operators with x subscript are applied to the test points.

The approach based on the interpolation formula of equation (8) is known as the Hermitian (or symmetric) method, producing a collocation matrix which is symmetric, and was shown by Wu [39, 50] to be non-singular provided that no two collocation points sharing a linearly dependent operator are placed at the same location. The Hermitian RBF approach has also been applied to a variety of problems within the literature [12, 51, 52], however Kansa's method remains the most commonly used method for solving PDEs with RBF collocation methods, primarily due to its flexibility and ease of implementation. A comparative analysis of the Kansa and Hermitian methods for steady convection-diffusion problems is given in [53].

Equation (8) will form the foundation of our local Hermitian interpolation (LHI) method, where for simplicity the L operator will be henceforth referred to as the PDE operator and B as the boundary operator. The flexibility of the full-domain Hermitian method to enforce multiple linearly independent boundary operators at a single location (known as double collocation; see [54]) is maintained within our LHI approach.

3 The LHI method for linear PDEs

The solution space Ω is covered by a set of (potentially) scattered data centres, as shown in Figure 1. These data centres represent the locations at which the solution value will be enforced within the interpolation function. Data centres are also placed on all boundary surfaces Γ, and at these locations the value of the boundary operator, B, is enforced. In addition, each local system has associated with it a series of locations at which the PDE governing operator, L, is applied. The flexibility of the RBF Hermitian method to allow multiple distinct operators to be applied at a single location can be exploited to allow placement of these PDE centres at the same location as solution centres, however previous investigations have indicated that a staggered placement of data centres is preferable in most cases [24]. In principle, the solution and boundary centres can be viewed as global objects, whereas the PDE centres can be viewed as locally defined objects which are associated with one or more local systems.

Each solution centre has associated with it a stencil of other nearby solution centres. If a stencil is sufficiently close to the boundary then the points at the intersection between the boundary and the stencil are included (see Figure 1), and where present the PDE centres are included also. Each stencil is used to perform a local interpolation; referred to henceforth as a local system. Local systems are not formed around boundary and PDE centres.

The solution field is approximated via a series of Hermitian interpolations on each of the local systems, using the functional values for solution centres, the source term values for PDE-operator centres, and the boundary operator values at boundary centres, in those cases where they are required. As with

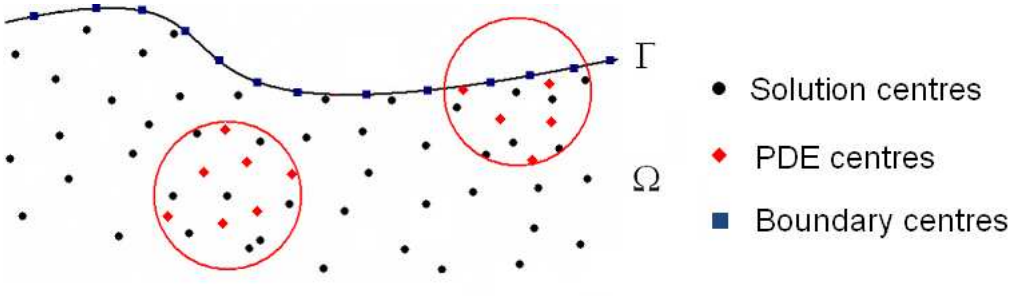

Figure 1: Schematic representation of local systems

the full-domain Hermitian method, the various operators are applied to the basis functions at their respective trial points. A polynomial term is included to complete the underlying vector space, as with equation (8).

In this way, at each local system the field variable is approximated by

$$\begin{aligned} u^{(k)}(x) &= \sum_{j=1}^{N_s} \alpha_j^{(k)} \Psi\left(\|x-\xi_j\|\right) + \sum_{j=N_s+1}^{N_s+N_B} \alpha_j^{(k)} B_\xi \left[\Psi\left(\|x-\xi_j\|\right)\right] \\ &+ \sum_{j=N_s+N_B+1}^{N_s+N_B+N_{PDE}} \alpha_j^{(k)} \bar{L}_\xi \left[\Psi\left(\|x-\xi_j\|\right)\right] + \sum_{j=1}^{NP} \alpha_{j+N} P_{m-1}^j(x) \end{aligned} \tag{10}$$

where

k	is the local system index
N_s	is the number of solution centres in the local system
N_B	is the number of boundary centres in the local system
N_{PDE}	is the number of PDE centres in the local system
NP	is the number of terms in a 3D polynomial of degree $m-1$

Consider a local Hermitian interpolation of a general scalar field, $u(x)$, which satisfies a PDE operator $\overline{L}$ in the domain Ω, and a boundary operator B at the boundary Γ, with values of the scalar field and operators given at a discrete set of points, as outlined in Figure 1.

$$\begin{aligned} \overline{L}\left[u(x)\right] &= S(x) \quad \text{in } \Omega \\ u(x_i) &= f_i \quad \text{in } \Omega \\ B\left[u(x)\right] &= g(x) \quad \text{on } \Gamma \end{aligned} \tag{11}$$

Here, the scalar values f_i will correspond to the unknown solution values within the computational domain Ω. This description can be collocated at each of the points within the local systems, $\Omega^{(k)}$, described by equation (10), applying once again the B operator at boundary centres and the L operator at the PDE centres. This leads to a series of small symmetric linear systems which can be solved

independently to interpolate the solution over the domain in a piecewise fashion. Therefore, a series of local systems

$$A^{(k)}\alpha^{(k)} = d^{(k)} \tag{12}$$

are constructed for the interpolation coefficients $\alpha^{(k)}$, where

$$A^{(k)}= \begin{bmatrix} \Psi_{ij} & B_\xi\left[\Psi_{ij}\right] & \overline{L}_\xi\left[\Psi_{ij}\right] & P_{m-1} \\ B_x\left[\Psi_{ij}\right] & B_xB_\xi\left[\Psi_{ij}\right] & B_x\overline{L}_\xi\left[\Psi_{ij}\right] & B_x\left[P_{m-1}\right] \\ \overline{L}_x\left[\Psi_{ij}\right] & \overline{L}_xB_\xi\left[\Psi_{ij}\right] & \overline{L}_x\overline{L}_\xi\left[\Psi_{ij}\right] & \overline{L}_x\left[P_{m-1}\right] \\ P_{m-1}^T & B_\xi\left[P_{m-1}\right]^T & \overline{L}_\xi\left[P_{m-1}\right]^T & 0 \end{bmatrix} \text{ and } d^{(k)} = \begin{bmatrix} f_i \\ g_i \\ S_i \\ 0 \end{bmatrix} \tag{13}$$

and where $\Psi_{ij} = \Psi\left(\|x_i - \xi_j\|\right)$ for points contained in local system k, ordered as indicated in equation (10).

In this way the value of u close to point k can be written as

$$u^{(k)}\left(x\right) = H\left(x\right)^{(k)}\alpha^{(k)} \tag{14}$$

where

$$H\left(x\right)^{(k)} = \left[\ \Psi\left(x-\xi_j\right),\quad B_\xi\left[\Psi\left(x-\xi_j\right)\right],\quad \overline{L}_\xi\left[\Psi\left(x-\xi_j\right)\right],\quad P_{m-1}\ \right] \tag{15}$$

By inverting the matrix system (13), i.e. $\alpha^{(k)} = \left[A^{(k)}\right]^{-1} d^{(k)}$, it is possible to express the field variable u at any point within the stencil of local system k in terms of the data vector $d^{(k)}$, i.e.

$$u^{(k)} = H\left(x\right)^{(k)}\left[A^{(k)}\right]^{-1} d^{(k)} \tag{16}$$

Similarly, any partial differential operator, Q, can be applied to the reconstruction vector $H^{(k)}$ in order to reconstruct the partial derivatives of the interpolated function:

$$\begin{aligned} Q\left[u^{(k)}\left(x\right)\right] &= Q\left[H^{(k)}\right]\alpha^{(k)} \\ &= \left[\ Q_x\left[\Psi\left(x-\xi_j\right)\right],\quad Q_xB_\xi\left[\Psi\left(x-\xi_j\right)\right],\quad Q_x\overline{L}_\xi\left[\Psi\left(x-\xi_j\right)\right],\quad Q_x\left[P_{m-1}\right]\ \right]\alpha^{(k)} \end{aligned} \tag{17}$$

As before, by expressing the vector $\alpha^{(k)}$ in terms of the data vector $d^{(k)}$, the value of the differential operator can be given by

$$\begin{aligned} Q\left[u^{(k)}\left(x\right)\right] &= Q\left[H^{(k)}\left(x\right)\right]\alpha^{(k)} \\ &= \left(Q\left[H^{(k)}\left(x\right)\right]\left[A^{(k)}\right]^{-1}\right) d^{(k)} \\ &= W_Q^{(k)}\left(x\right) d^{(k)} \end{aligned} \tag{18}$$

where $W_Q^{(k)}$ is a *stencil weights* vector for the differential operator Q at local system k. The stencil weights vector $W_Q^{(k)}$ can also be obtained via the solution of a linear system, avoiding the need to

explicitly calculate and store the local matrix inverse:

$$\begin{aligned}\left(Q\left[H^{(k)}\right]\right)\left[A^{(k)}\right]^{-1} &= W_Q^{(k)} \\ Q\left[H^{(k)}\right] &= \left[A^{(k)}\right]^T W_Q^{(k)} \\ &= A^{(k)} W_Q^{(k)} \quad \text{(exploiting symmetry)}\end{aligned} \tag{19}$$

In most cases LU-factorisation will be the most computationally efficient method of solution for these small linear systems, as the LU factors can be re-used to obtain stencil weight vectors for any additional operators, at a cost of $o\left(N^2\right)$ floating point operations.

3.1 Solution of steady problems

For a steady PDE:

$$\begin{aligned}\overline{L}\left[u\left(x\right)\right] &= S\left(x\right) \qquad \text{in}\,\Omega \\ B\left[u\left(x\right)\right] &= g\left(x\right) \qquad \text{on}\,\Gamma\end{aligned} \tag{20}$$

With $A^{(k)}$ as indicated in equation (13), the data vector becomes

$$d^{(k)} = \begin{bmatrix} u_i \\ g_i \\ S_i \\ 0 \end{bmatrix} \tag{21}$$

with $f_i = u_i$, representing the unknown values of $u\left(x\right)$ at the local solution centres, and the rest of the data vector composed of known quantities.

By applying the PDE operator $\overline{L}\left[u\right] = S\left(x\right)$ to a reconstruction vector at the central point of the local system, i.e. by setting $Q = \overline{L}$ in equation (18), a relation can be obtained linking the values of u_i within the local system

$$\begin{aligned}S\left(x_{centre}\right) &= \overline{L}\left[u^{(k)}\left(x_{centre}\right)\right] \\ &= W_{\overline{L}}^{(k)}\left(x_{centre}\right) d^{(k)}\end{aligned} \tag{22}$$

Applying the above reconstruction to each local system k, a series of N simultaneous equations are produced for $u_i,\ i = 1, \ldots, N$, where N is the global number of solution centres. In the resulting global linear system the corresponding boundary conditions of the problem have already been imposed, at the local interpolation, in those stencils containing boundary points. This sparse linear system of equations can be solved efficiently using standard solution techniques for sparse linear systems.

3.2 Solution of time dependent problems

The method of solution for time dependent problems requires the creation of a modified PDE-operator via a finite difference approximation of the time derivative. The procedure is illustrated here using a Θ-weighted Crank-Nicolson approach, but is easily extensible to any number of finite difference time advancement schemes.

For a general initial-boundary value problem

$$\begin{array}{rcll} \dfrac{\partial u(x,t)}{\partial t} & = & L[u(x,t)] + S_2(x,t) & \text{in } \Omega \\ u(x,0) & = & f(x) & \text{in } \Omega \\ B[u(x,t)] & = & g(x,t) & \text{on } \Gamma \end{array} \tag{23}$$

a finite difference approximation is made to the time-derivative

$$\frac{u^n - u^{n-1}}{\Delta t} = \Theta L[u^n] + (1-\Theta) L\left[u^{n-1}\right] + S_2(x,t^n) \tag{24}$$

From this approximation, a modified PDE operator is obtained

$$\overline{L}[u^n] = \hat{L}\left[u^{n-1}\right] + S_2(x,t^n) \tag{25}$$

where

$$\begin{array}{rcl} \overline{L} & = & 1 - \Theta \Delta t\, L \\ \widehat{L} & = & 1 + (1-\Theta)\Delta t\, L \end{array} \tag{26}$$

The time stepping algorithm implies that the original initial boundary value problem reduces at each time step to the solution of a boundary value problem defined by the non-homogeneous partial differential equation (25), with the non-homogeneous term given in terms of the solution of the problem at the previous time step. At this stage the formulation at a given time step is identical to the formulation for steady problems, assuming that $\hat{L}\left[u^{n-1}\right]$is known from interpolation at the previous time step. $S(x) = \hat{L}\left[u^{n-1}\right] + S_2(x,t^n)$ is taken as the equivalent to the non-homogeneous term of the PDE in equation (20). As such the solution procedure at each time step is performed in the same way as for the steady problem, using the modified operator and the corresponding non-homogeneous term.

After solution of the global linear system, and using the current interpolation matrix systems and updated data-vectors, a reconstruction of $\hat{L}[u^n]$ at the solution and PDE centres must be made, ready for the calculation of $S(x)$ at the next time step. This is done via the creation of further reconstruction arrays

$$\begin{array}{rcl} \hat{L}[u^n(x_i)] & = & \hat{L}\left[H^{(k)}(x_i)\right]\alpha^{(k)} \\ & = & W_{\hat{L}}^{(k)}(x_i)\, d^{(k)} \end{array} \tag{27}$$

for every x_i at which the reconstruction is required, within local system k; i.e. setting $Q = \widehat{L}$ in equation (18).

The initial time step is always performed using the $\Theta = 1$ first-order implicit time stepping formulation. Were a value of $\Theta < 1$ to be used, $L\left[u^0\right]$ would be required in order to calculate the S_i which appear

in the local system data vector of equation (21). This quantity is unknown at the initial configuration, and in order to be calculated would require an interpolation of the initial solution field, using a different interpolation system which does not rely on a non-existent previous time step. At subsequent time steps any value of Θ can be chosen without altering the interpolation system. For more detail on the LHI formulation for linear problems, including the performance of different stencil sizes and configurations, and methods for minimising storage and computational cost, see [24]. For a procedure to accurately capture discontinuities in governing PDE properties, for example at material interfaces, see [55].

3.3 Shape parameter

It is worth noting that the value of the multiquadric shape parameter, c, has not been explicitly defined (see equation (1)). The shape parameter represents a local lengthscale, and as such, with the local interpolation systems of the LHI method it is more natural to define the non-dimensionalised shape parameter

$$c^* = \frac{c}{\Delta_{max}} \tag{28}$$

where Δ_{max} is the separation from the local system centrepoint to the most distant point included in the system. This allows variations in Δ_{max} within a dataset to be accounted for. Determination of an optimal value of c^* is a nontrivial issue, and requires further research for local RBF methods.

Certainly, the conditioning of the local system matrices (13) has a significant impact on the selection of c^*. Larger values of c^* will produce increasingly ill-conditioned local system matrices, and as such the range of allowable c^* is limited by the nature of the local matrices; specifically the number, location and type of data centres, and the precision of the arithmetic used. Many authors examine the condition number of the local system matrices and adjust the shape parameter to match a target maximum conditioning value (see for example [56]). However, it can be shown that the optimal value of the shape parameter is also dependent on the nature of the data to be interpolated (see [57] or [58] for analysis with full domain RBF methods, or [25] for an example with the LHI method). The optimal c^* value is not always the maximum value allowed by the local matrix conditioning, and may be required to vary over the solution domain in order to obtain an optimal solution. In particular, with problems which feature rapid changes in gradient or other near-discontinuous features within an interpolation system smaller values of c^* may be preferable.

In the current work, a suitable value of c^* is selected for each of the two problems examined, and is used for all configurations tested within that problem. The value of c^* is not optimised to minimise the solution error, as to do so would require a different value of the shape parameter for each configuration and perhaps each timestep. In more practical problems where analytical solutions are not available, it is possible to extract information about local solution quality by examining the local PDE residual, at locations other than the data centres (at which the governing PDE is enforced and the residual will necessarily be zero). By varying the shape parameter it is possible to reduce the value of the residual, which may lead to an improved solution reconstruction. However, such an optimisation of the shape parameter is expensive, and there is no guarantee that the value of c^* which minimises the residual will also minimise the solution error, particularly with steady problems (as has been observed experimentally by the authors).

Any further investigation into efficient techniques for data-dependent shape parameter optimisation with local RBF methods would be a welcome addition to the field of research.

4 The LHI method for heat-transfer problems

The conduction of heat in isotropic materials having temperature-dependent thermal properties, with an arbitrary body source, is given by equation (29); see [59]:

$$\rho\left(T\right)C_{p}\left(T\right)\frac{\partial T}{\partial t}=\frac{\partial}{\partial x_{i}}\left(k\left(T\right)\frac{\partial T}{\partial x_{i}}\right)+s\left(x_{i},t\right) \tag{29}$$

where

T	is the temperature
ρ	is the material density
C_p	is the specific heat capacity
k	is the thermal conductivity

The temperature-dependent variation of density and specific heat capacity can be combined into the volumetric heat capacity; $c_{v}\left(T\right)=\rho\left(T\right)C_{p}\left(T\right)$.

4.1 Kirchhoff transformation

The Kirchhoff integral transformation is applied, in order to reduce the degree of nonlinearity in the governing equation (29).

the Kirchhoff transformation is taken as:

$$\psi\left(T\right)=\int_{T_{0}}^{T}k\left(\chi\right)d\chi \tag{30}$$

By applying the Kirchhoff transformation to the temperature, equation (29) can be rewritten as:

$$\frac{\partial\psi}{\partial t}=\frac{k\left(\psi\right)}{c_{v}\left(\psi\right)}\left(\frac{\partial^{2}\psi}{\partial x_{i}^{2}}+s\left(x_{i},t\right)\right) \tag{31}$$

The transformation of the nonlinear diffusion term into Kirchhoff space reduces the equation from a strongly nonlinear to a weakly nonlinear form, by removing the multiplication of first derivatives in the diffusive term::

$$\begin{aligned}\frac{1}{c_{v}\left(T\right)}\frac{\partial}{\partial x_{i}}\left(k\left(T\right)\frac{\partial T}{\partial x_{i}}\right) &= \frac{1}{c_{v}\left(T\right)}\left[k\frac{\partial^{2}T}{\partial x_{i}^{2}}+\frac{dk}{dT}\left(\frac{\partial T}{\partial x_{i}}\right)^{2}\right] && \text{Strongly nonlinear}\\ &= \frac{1}{c_{v}\left(T\right)}\frac{\partial^{2}\psi}{\partial x_{i}^{2}} && \text{Weakly nonlinear}\end{aligned} \tag{32}$$

The 'price' for this reduction in nonlinearity is the necessity to obtain a closed-form representation of $\psi\left(T\right)$ and its inverse function $T\left(\psi\right)$, as well as for the two functions $k\left(\psi\right)$ and $c_{v}\left(\psi\right)$. Since the thermal conductivity $k\left(T\right)$ is usually known only as a series of pointwise measurements, the accurate computation of these functions can be nontrivial. A variety of interpolation methods can be used, with the two most popular methods within the literature being piecewise linear interpolation, or the use of

a global polynomial (see for example [32] and [60]). An alternative is the use of RBF interpolation and numerical integration in order to obtain the required functions $\psi(T)$, $k(\psi)$, $c_v(\psi)$ and $T(\psi)$. The procedure for obtaining such functions with RBF interpolation is described in 6.

Boundary conditions must also be transformed to Kirchhoff-space:

$$\begin{array}{lllll} \text{Dirichlet:} & T(x,\,t) = f(x,\,t) & \Rightarrow & \psi(x,\,t) = \psi(f(x,\,t)) \\ \text{Neumann:} & n_i \dfrac{\partial T}{\partial x_i} = g(x,\,t) & \Rightarrow & n_i \dfrac{\partial \psi}{\partial x_i} = k(\psi)\, g(x,\,t) \end{array} \tag{33}$$

The transformation takes a linear Neumann condition in temperature-space to a nonlinear condition in Kirchhoff-space. However, in practice, the direct application of temperature gradient Neumann conditions is rare; heat-flux boundary conditions are much more commonly applied. The surface heat flux $q_s(x,t)$ is given by (see [59]):

$$\begin{aligned} q_s(x,\,t) &= -n_i\, k(T) \frac{\partial T}{\partial x_i} \\ &= -n_i \frac{\partial \psi}{\partial x_i} \end{aligned} \tag{34}$$

In this case the transformation to Kirchhoff space removes the nonlinearity in the boundary condition; a nonlinear heat-flux condition in temperature-space is reduced to a linear Neumann condition in Kirchhoff-space (see equation (34)).

4.2 Solution procedure

The solution to the nonlinear equation (31) cannot be obtained directly, requiring instead a process of nonlinear iterations. The current solution procedure performs Picard iterations on the Kirchhoff transform variable and functions thereof, in order to iteratively approach the solution at each timestep.

An approximation is taken to the Kirchhoff transform variable ψ, written henceforth as $\widetilde{\psi}$. From this, the current guess-values of $\widetilde{k} = k\left(\widetilde{\psi}\right)$ and $\widetilde{c_v} = c_v\left(\widetilde{\psi}\right)$ can be obtained. Both of these quantities are required at the solution and PDE data centres, and $\widetilde{k}$ is required at the Neumann boundary centres. Within the nonlinear iteration these quantities are considered constant, leading to the linearised equation:

$$\frac{\partial \widetilde{\psi}}{\partial t} = \frac{\widetilde{k}}{\widetilde{c_v}} \left(\frac{\partial^2 \widetilde{\psi}}{\partial x_i \partial x_j} + s(x_i, t) \right) \tag{35}$$

This equation can be solved directly, using the procedure outlined in section 3. The contribution from the effective body source term, $\frac{\widetilde{k}}{\widetilde{c_v}} s(x_i,\, t)$, is taken account as an addition to the right-hand-side of the global matrix system, and also to the local data vector where the PDE governing operator is applied (i.e. the PDE centres). Convergence is examined by comparing the maximum change in $\widetilde{\psi}$ over the nonlinear iteration against a user specified convergence parameter ϵ_{NL}. Once convergence has been reached, the $\hat{L}\left[\widetilde{\psi}^n\right]$ quantity (see equation (25)) can be reconstructed ready for the next time step.

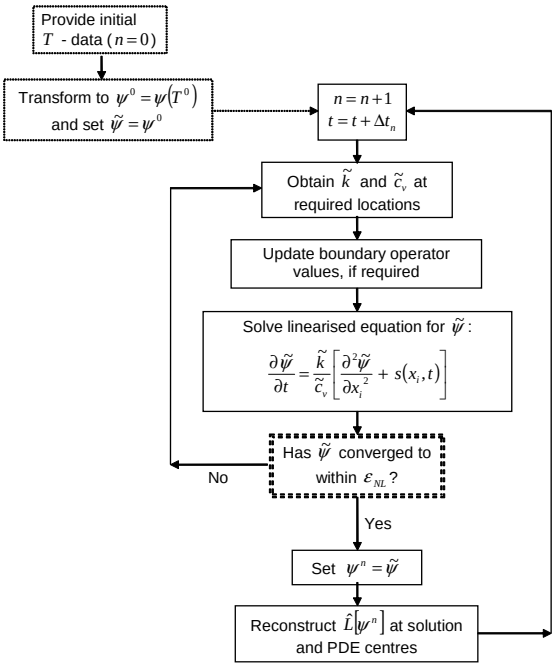

Figure 2: Schematic description of the nonlinear solution procedure

This procedure is summarised in Figure 2. The procedure for steady problems is similar, except for the absence of the time-advancement loop and the $\hat{L}\left[\widetilde{\psi^n}\right]$ reconstruction.

Note that for steady problems the initial guess variable $\widetilde{\psi_0}$ is required only at the boundaries. For Dirichlet boundary conditions the guess value is the transformation of the imposed Dirichlet value (see equation (33)). For temperature-gradient Neumann boundaries, a guess value of $\widetilde{\psi}$ is needed in order to compute $\widetilde{K_r}$. For the first iteration a guess value of $\widetilde{\psi} = 0$ will usually suffice, however on subsequent iterations this value must be reconstructed from the surrounding solution field in order for the Neumann boundary operator to converge on the correct value. For transient problems the initial guess value of $\widetilde{\psi}$ is required at all solution, PDE and boundary centres, and is obtained directly from the transformed initial solution field.

5 3D validation case

A nonlinear heat conduction problem is formulated in a hypothetical material with known thermal properties, using a mixture of Dirichlet and Neumann temperature-gradient boundary conditions.

Taking

$$\begin{aligned} k(T) &= T \\ c_v(T) &= 1 \\ s(x,\, t) &= -3 - (6 + \lambda r)\, e^{-\lambda t} - 3e^{-2\lambda t} \end{aligned} \tag{36}$$

with α and λ as arbitrary scalar parameters, the governing equation (29) becomes

$$\frac{\partial T}{\partial t} = \frac{\partial}{\partial x_i}\left(T\frac{\partial T}{\partial x_i}\right) - 3 - (6 + \lambda r)\, e^{-\lambda t} - 3e^{-2\lambda t} \tag{37}$$

which has an analytical solution given by:

$$T(x,\, t) = r\left(1 + \alpha e^{-\lambda t}\right) \tag{38}$$

At the origin, the value of the thermal conductivity becomes zero, and as such the solution becomes singular at this location.

The computational domain is considered to be a cuboid, represented by $x \in [x_{min},\, x_{max}]$, $y \in [y_{min},\, y_{max}]$, $z \in [z_{min},\, z_{max}]$. The analytical solution field 38 is applied at the x_{max}, y_{max} and z_{max} boundaries as a Dirichlet boundary condition. The gradient of the analytical temperature field is imposed at the x_{min}, y_{min} and z_{min} boundaries, i.e.

$$n_i \frac{\partial T}{\partial x_i} = \frac{n_i\, x_i}{r}\left(1 + \alpha e^{-\lambda t}\right) \tag{39}$$

where n_i represents the surface normal at the boundary. At the locations where the Neumann boundaries converge, each of the converging temperature gradient conditions is imposed simultaneously, taking advantage of the double collocation property of the RBF Hermitian method. As described in section 4.1, the application of (linear) temperature-gradient boundary conditions leads to a nonlinear boundary condition in the Kirchhoff-transformed governing equation. The use of temperature-gradient Neumann boundaries in this problem allows the transformation procedure to be validated. The initial condition is obtained by applying the analytical solution (38) over the interior of the solution domain, at $t = 0$.

Two separate domains are examined. The first domain takes $x_{min} = y_{min} = z_{min} = 0$, and $x_{max} = y_{max} = z_{max} = 2$. As such, the singularity at the origin is included within each of the three Neumann boundaries of the problem. However, the normal gradient of the temperature at each of these three Neumann surfaces is considered to be zero at the origin, where the singularity lies. This can be considered valid, since the temperature gradient is analytically zero over each of these three surfaces in the limit $r \to 0$. The second domain takes $x_{min} = y_{min} = z_{min} = 1$, and $x_{max} = y_{max} = z_{max} = 3$, leading to a nonsingular solution throughout the domain, and a non-zero temperature gradient over each of the Neumann boundaries. The two domains described above will be henceforth referred to as the *singular* and the *translated* domains respectively.

The solution domain is discretised using a uniform distribution of $(11 \times 11 \times 11)$ solution and boundary centres. Local systems are formed by connecting each of the solution centres to each solution or boundary centre within a single Cartesian index of itself, leading to a stencil of 27 solution or boundary

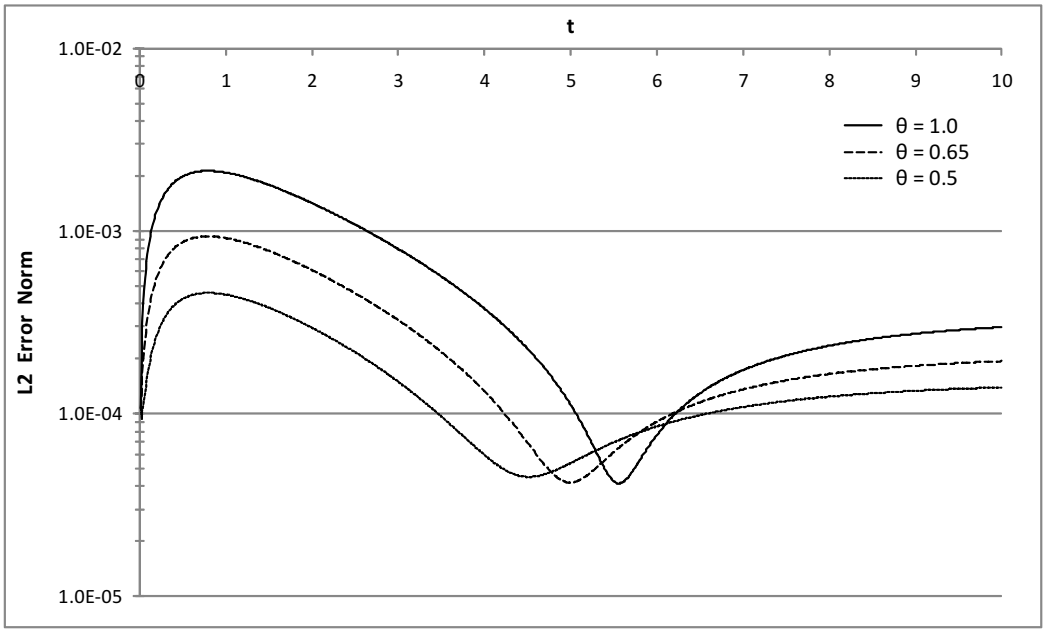

Figure 3: Variation of L_2 error norm with runtime : Singular case

centres. PDE centres are additionally placed at every Cartesian half-index, leading to 8 PDE centres within each local stencil. A non-dimensionalised shape parameter of value $c^* = 5$ is used throughout. The value of the parameters α and λ are both taken to be 0.5. For the transient case, local systems are reformed after every timestep. For the steady case local systems are reformed after every nonlinear iteration. In both cases, the convergence parameter is taken to be $\epsilon_{NL} = 10^{-6}$ in the L_∞ norm. For the transient case a timestep of size $\Delta t = 0.01$ is used, with a variety of time advancement schemes.

Figure 3 shows the variation of the (absolute) L_2 solution error with time, for the singular case, using three different time advancement schemes. In each case the profile of the error appears similar. The error rises rapidly from the initial condition, reaching its maximum value at around $t = 0.6$. From here the error decreases towards a minimum value at around $t = 5$, before rising again towards a steady value. The second-order $\Theta = 0.5$ time advancement scheme offers the best accuracy overall, with the first-order $\Theta = 1$ scheme providing the least accurate solution for most runtimes. The $\Theta = 0.65$ mixed scheme offers accuracy intermediate to the other two schemes.

Figure 4 shows the equivalent error variations for the translated case. Here the accuracy is significantly improved for each of the time advancement schemes, in comparison to the singular case. This is most likely a consequence of the singularity not being present within the solution domain; with the singular case the maximum error is always found at the solution centre closest to the singularity, whereas with the translated case the maximum error location may change as the solution progresses. Once again, the $\Theta = 0.5$ case provides the most accurate solution and the $\Theta = 1$ scheme the least accurate, with the $\Theta = 0.65$ scheme offering intermediate accuracy. The error profile appears similar to the singular case, with the main difference being that the peak error is achieved at a much earlier runtime (around $t = 0.2$). In both the singular and translated cases, the solution is replicated to a high degree of

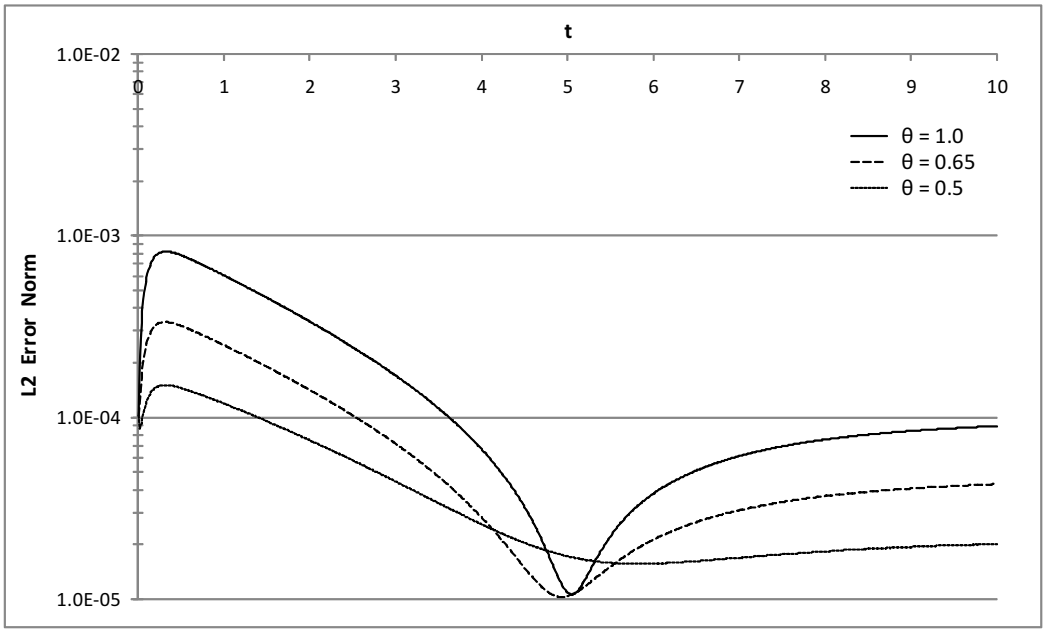

Figure 4: Variation of L_2 error with runtime : Translated case

accuracy throughout the time advancement procedure.

When the steady solution is obtained directly, using the steady solution procedure, the L_2 error at the solution centres is 1.49×10^{-3} for the singular case, and 3.44×10^{-4} for the translated case. As such, it appears that approaching the steady solution using any of the transient solution schemes offers a higher degree of accuracy than can be achieved by using the steady solution procedure, when a consistent shape parameter value is used. As is the case with many other problems, it was informally observed that alteration of the shape parameter value has a more significant effect on the accuracy of the steady case than it does on the transient case. However, for consistency a single representative shape parameter is used for all configurations.

6 Interpolation and transformation of thermal property data

As indicated in section 4.1, the Kirchhoff transformation can be employed to significantly reduce the degree of nonlinearity in the nonlinear heat equation. However, this transformation also requires the thermal conductivity and volumetric heat capacity, k and c_v, to be transformed from functions of temperature into functions of the Kirchhoff variable. In most practical cases these material functions do not have a closed-form functional representation, and are known only via pointwise experimental data. As such, the transformation to Kirchhoff space cannot be made directly. It may be possible to interpolate the material curves $k(T)$ and $c_v(T)$ by using global polynomial functions (see for example [60]). However, in many cases experimental data can not be approximated well by a low-order polynomial, and as such a polynomial of high order is often required. Such a high-order polynomial

will often exhibit undesirable oscillations; the well known "polynomial snaking effect".

In cases where a global polynomial representation is not viable, it is logical to recourse to piecewise interpolation of the available experimental data. One possibility is to use a linear or piecewise-constant representation of the material functions. Such interpolation leads to at most a quadratic local approximation for the Kirchhoff variable, and hence the conversion back to the original variable (temperature) is relatively simple to obtain analytically. An alternative to such piecewise interpolation is to use a global 1D radial basis function interpolation. Since radial basis function methods can exhibit exponential convergence rates with interpolation problems [3], such methods may offer a high resolution alternative to piecewise polynomial interpolation. The procedure for the transformation of material properties to Kirchhoff space is outlined here:

The values of $k(T)$ and $c_v(T)$ are entered at a set number of sample points, T_j, as determined by the available experimental data. A traditional RBF interpolation is then performed on the data (see section 2) in order to obtain the interpolation functions; $\overline{k}(T)$ and $\overline{c_v}(T)$. From the interpolation function $\overline{k}(T)$ a numerical integration can be performed to obtain an estimate of the Kirchhoff transformation, ψ_j, at the original sample points. The procedure currently implemented by the LHI numerical software samples $\overline{k}(T)$ at 5 locations within each sample point interval, in order to perform a 9^{th}-order Gauss-Legendre integration between each pair of sample points.

The discrete representation of ψ_j can then be used to obtain RBF interpolations for both the Kirchhoff transform and its inverse; $\overline{\psi}(T)$ and $\overline{T}(\psi)$ respectively. With the continuous functions for $\overline{\psi}(T)$ and $\overline{T}(\psi)$ now available, the transformed functions $\overline{k}(\psi)$ and $\overline{c_v}(\psi)$ can be obtained in much the same fashion; by sampling the available interpolations of $\overline{k}(T)$ and $\overline{c_v}(T)$ at the locations corresponding to the data centres of ψ (i.e. ψ_j as previously defined), and performing an RBF interpolation.

Although it is necessary to form and solve an RBF interpolation system for $\overline{k}(\psi)$ and $\overline{c_v}(\psi)$ during the problem setup phase, the computational cost to extract data for any of the functions is fairly small, requiring only the formation of a reconstruction array and its multiplication with a stored solution vector. This comes at a computational cost of $o(M)$ operations for every reconstruction, where M is equal to the number of data sample points. This cost will be significantly less than the cost of the solution procedure described in section 4, unless M is much larger than the size of the local systems.

To give an indication of the level of accuracy which could be expected from a 1D RBF interpolation procedure, the following simple numerical example is formulated. A hypothetical model for $k(T)$ and $c_v(T)$ is examined, which has a known Kirchhoff transformation; see equation (40).

$$\begin{aligned} K_r &= \left(\frac{T}{100}\right)^{-2.0} \\ c_v(T) &= 0.1 + 0.5\left(\frac{T}{100}\right)^{-1.5} \end{aligned} \tag{40}$$

The material data is chosen such that it varies relatively rapidly, and as such present a reasonable challenge to accurate and stable interpolation. It is expected that most physical materials will not experience such large changes in magnitude, or such rapid rates of decay, over typical operational temperature ranges. A temperature range of $100 \leq T \leq 1000$ is studied in this case. The values of k and c_v are sampled with two datasets, utilising 31 and 16 sample points respectively, with the sample set refined slightly as $T = 100$ is approached. The sample locations for the 16-point dataset

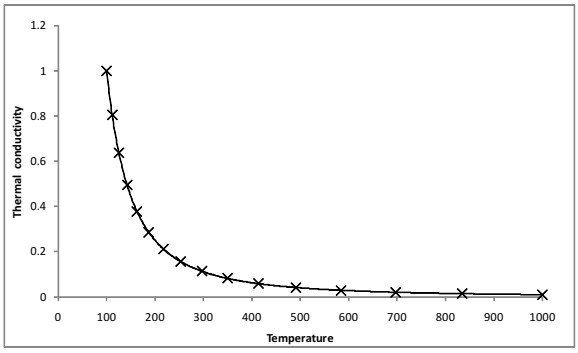

(a) Thermal conductivity $k(T)$

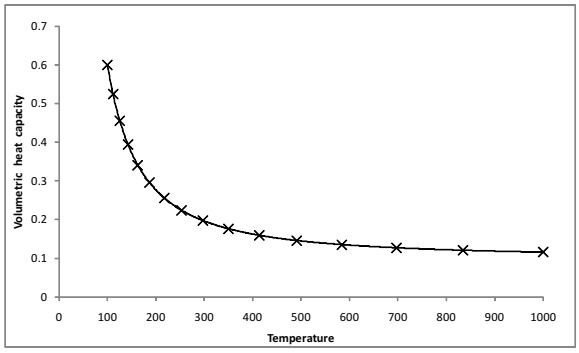

(b) Volumetric heat capacity $c_v(T)$

Figure 5: Material curves used for interpolation. Crosses represent the location of the data centres in the coarse sample set

	16 sample points (relativeL_2 error)	31 sample points (relativeL_2 error)
$k(\psi)$:	4.02×10^{-3}	1.01×10^{-3}
$c_v(\psi)$:	4.29×10^{-3}	1.08×10^{-3}
$\overline{T}\left(\overline{\psi}(T)\right)$	1.04×10^{-4}	8.22×10^{-5}

Table 2: Relative L_2 error norms in the reproduction of Kirchhoff-transformed functions

are marked on Figure 5, and the 31-point dataset places an additional sample point at the mid-point of each interval.

With the interpolation procedure described above it is possible to choose a reasonable shape parameter by examining the error in transforming to the Kirchhoff variable and back again; i.e. by examining the value of $\left[\overline{T}\left(\overline{\psi}\left(\ddot{T}_i\right)\right) - \ddot{T}_i\right]$ at a large number of reconstruction locations $\ddot{T}_i$, and choosing a shape parameter which minimises this quantity in some norm. Here the L_2-minimising shape parameter is automatically utilised. Since only two RBF interpolation systems are required during problem setup, the cost of analysing even many hundreds of shape parameters is still negligible for reasonably sized datasets.

Table 2 shows the relative L_2 error norms found in the required Kirchhoff functions, $\overline{k}(\psi)$ and $\overline{c_v}(\psi)$, as measured at 1001 uniformly spaced reconstruction locations over the range of ψ. In addition, the relative L_2 norm of the quantity $\left[\overline{T}\left(\overline{\psi}\left(\ddot{T}_i\right)\right) - \ddot{T}_i\right]$ is reported, as measured at 1001 uniformly spaced $\ddot{T}_i$ over the range of T. The error in this quantity is very small with both datasets, as can be expected due to its optimisation via the shape parameter (see Table 2). The magnitude of the error in the transformed functions is also reasonably small, and appears to respond well to the addition of further discretisation points. Considering that these functions have been subjected to two separate interpolations and, indirectly, a numerical integration procedure, the observed relative error of between 0.1% and 0.4% can be considered to be good.

T (K)	k (W $m^{-1}K^{-1}$)	c_v (J K^{-1} m^{-3})
100	33.2	1.35×10^6
200	25.2	1.73×10^6
400	21.6	1.97×10^6
600	20.7	2.12×10^6
800	21.6	2.25×10^6
1000	23.7	2.38×10^6
1200	26.0	2.26×10^6

Table 3: Material properties for zirconium

7 Full-domain RBF comparison case

The following numerical example replicates a test case from the literature (see [32]), which has been solved using the full-domain Kansa RBF collocation method (see section 2), with the Kirchhoff transformation applied and a piecewise-linear interpolation performed to transform the variable to Kirchhoff space. In [32] the case is solved in 2D on a coarse dataset, however in the present example an equivalent 3D solution is obtained, with zero temperature-gradient conditions applied at the z boundaries in order to replicate a 2D solution. This allows a direct comparison of solution accuracy with the results using the Kansa RBF method. In addition, a fully 3D numerical example is presented using a similar formulation. This numerical test case uses real material properties, with the Kirchhoff functions interpolated from pointwise experimental measurements using the RBF interpolation procedure.

The material properties for zirconium are taken, as measured at 7 temperature values (see Table 3). From these pointwise data values, the 1D RBF interpolation procedure is performed in order to obtain representations for c_v and k in Kirchhoff space. Since the variation of the material properties is smooth and the magnitude does not change dramatically with temperature, an accurate reconstruction of the continuous material functions can be expected with only a small sample dataset.

For consistency with the example presented in [32], the domain is taken as $x \in [0,\, 0.12\text{m}]$, $y \in [0,\, 0.12\text{m}]$, $z \in [0,\, 0.12\text{m}]$. The analytical solution is imposed as:

$$\overline{T}\,(x,\, y,\, t) = \left[104.43 + 4.43\cos\left(0.01t\right)\right] e^{10(x+y)} \tag{41}$$

This analytical solution is achieved by adjusting the body source term at each nonlinear iteration, via:

$$s\,(x,\, y,\, t) = c_v\left(\overline{T}\right)\frac{\partial \overline{T}}{\partial t} - \left(\frac{\partial^2 \overline{T}}{\partial x^2} + \frac{\partial^2 \overline{T}}{\partial y^2}\right) k\left(\overline{T}\right) - \left[\left(\frac{\partial \overline{T}}{\partial x}\right)^2 + \left(\frac{\partial \overline{T}}{\partial y}\right)^2\right] \left.\frac{\partial k}{\partial T}\right|_{T=\overline{T}} \tag{42}$$

In this way, the source term depends directly on the material property functions $c_v\,(T)$ and $k\,(T)$. The value of $\frac{dk}{dT}$ at the exact temperature $\overline{T}$ is obtained by extracting the derivative from the interpolated $k\,(T)$ function. It is important to note that the source term in this problem is highly artificial, and is directly dependent upon the interpolated value of the material functions k and $\frac{dk}{dT}$ in order to ensure that the enforced analytical solution is obtained. Hence, a more accurate reconstruction of the experimental data in Table 3 will not necessarily lead to a more accurate numerical solution. As such, in this

case, the high-resolution 1D RBF interpolation offers no benefit over the piecewise linear reconstruction of the material data which is used in [32]. In true physical examples however, where the analytical solution is not known and a physical body-source term is utilised, a more accurate representation of material properties should generally lead to a more physically representative numerical solution.

The imposed analytical solution $\overline{T}$ is used to provide the initial condition for the simulation, as well as the Dirichlet boundary condition imposed at the $x = 0.12$m, $y = 0$ and $y = 0.12$m boundaries. At the $x = 0$ boundary, the analytical solution is used to provide a suitable a heat-flux condition, i.e.

$$-k\left(T\right)\, n_i \frac{\partial T}{\partial x_i} = 10\, k\left(\overline{T}\right)\, \overline{T} \tag{43}$$

In order to retain a 2D solution for comparison with the results obtained in [32], a zero temperature-gradient Neumann condition is imposed at the $z = 0$ and $z = 0.12$m boundaries. The solution domain is discretised by placing solution and boundary data-centres with a uniform separation of $\Delta = 0.01$m. PDE centres are placed at every Cartesian half-index, and a stencil configuration of 27 solution or boundary centres and 8 PDE centres is utilised, as with the previous numerical example. A non-dimensionalised shape parameter of value $c^* = 5$ is used throughout.

In this case, a relative L_2 error norm is used to quantify the accuracy of the temperature profile in the numerical simulations;

$$\varepsilon = \left[\frac{1}{N}\sum_{i=1}^{N}\left(1 - \frac{T_i^n}{\overline{T}_i^n}\right)^2\right]^{\frac{1}{2}} \tag{44}$$

where the measurements T_i^n and $\overline{T}_i^n$ are taken from solution centre i at time step n, and N is the total number of solution centres.

In Figure 6 the variation of L_2 relative error, ε, is shown for the LHI method in 3D, and for the full-domain Kansa method in 2D as implemented in [32]. In both cases the runtime is taken as 500s, the timestep is taken as $\Delta t = 0.125$s, and a second order Crank-Nicholson time advancement method is used ($\Theta = 0.5$). It can be seen that the LHI method and the full-domain Kansa method both provide results of similar accuracy, with the LHI method offering slightly better accuracy for $t \lesssim 250$s, and the full-domain Kansa method offering slightly better accuracy for $t \gtrsim 250$s. In this case it was observed that the choice of time advancement scheme has very little effect on the solution quality, and that a much larger timestep can be used without a significant reduction in accuracy. For example, by using the first order $\Theta = 1$ scheme with a time step of $\Delta t = 1.0$s, the maximum difference in ε from the case presented in Figure 6 was observed to be is less than 5.0×10^{-5}. This implies that the error in this case is almost entirely a consequence of the spatial discretisation, and the accuracy of the body-source term approximation.

This test case is perhaps not the best with which to validate the performance of the method, given the artificial and solution-dependent nature of the body-source term. However it is sufficient to indicate that 3D performance of the LHI method is comparable to the 2D performance of the full-domain Kansa RBF collocation method, when using a coarse dataset. It is important to highlight once again that the LHI method, as with other local RBF methods, is capable of scaling to arbitrarily large datasets in 3D without computational cost or numerical conditioning issues. The full-domain Kansa RBF collocation method used in [32] exhibits, at best, order-N^2 computational complexity, and will suffer from numerical conditioning issues as the dataset size increases.

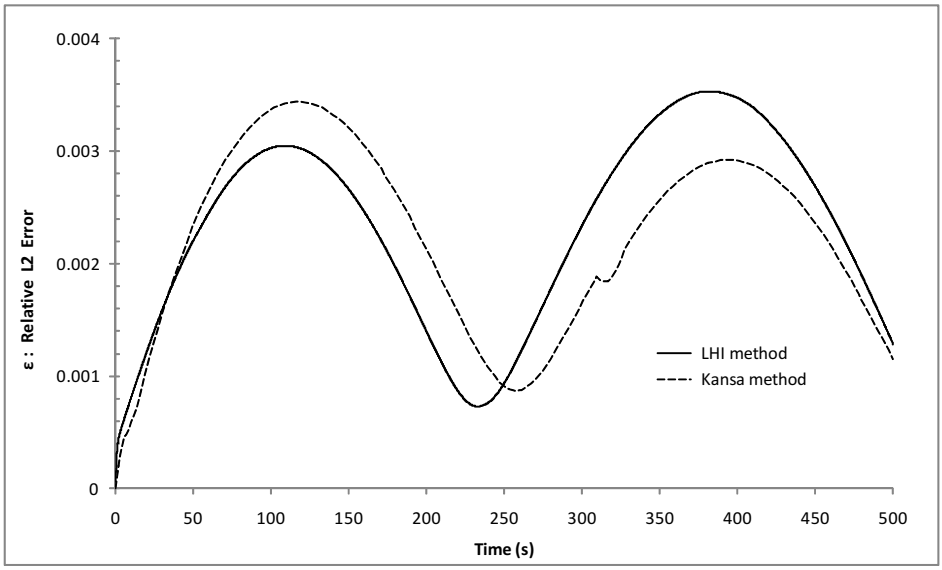

Figure 6: Variation of L_2 relative error with time: 2D test-case

A fully 3D version of the above example is also formulated. The following analytical solution is imposed, as a 3D equivalent of equation (41):

$$\overline{T}\left(x, y, z\, t\right) = \left[104.43 + 4.43\cos\left(0.01t\right)\right] e^{\frac{20}{3}(x+y+z)} \tag{45}$$

The solution domain remains the same, and the body-source term is once again generated via equation (42). The $x = 0$ heat-flux boundary and the $x = 0.12$m, $y = 0$ and $y = 0.12$m temperature boundaries are imposed in the same way as previously. However, in this case the the analytical solution $\overline{T}$ is additionally imposed at the $z = 0$ and $z = 0.12$m boundaries. The L_2 relative error profile for the 3D case is shown in Figure 7, once again using the $\Theta = 0.5$ time advancement scheme with $\Delta t = 0.125$. The error in this 3D case is significantly lower than that obtained from the 2D case presented in Figure 6. Unlike the 2D case the error profile does not appear to vary smoothly with time, however it does remain more consistent, providing an error of around $\varepsilon = 4.5 \times 10^{-4}$ throughout the simulation.

8 Conclusions

A formulation has been proposed to apply a meshless numerical method to heat conduction problems, where the material properties vary with temperature. The proposed numerical method, which is based on an Hermitian radial basis function collocation approach, allows arbitrary boundary operators to be imposed directly into the solution construction. Unlike traditional radial basis function collocation methods which use globally-supported interpolation systems, the proposed numerical technique uses a series of heavily overlapping local interpolation systems. This leads to order-N computational complexity, and allows scaling of the method to large datasets without the numerical ill-conditioning or computational complexity issues experienced by traditional RBF collocation techniques.

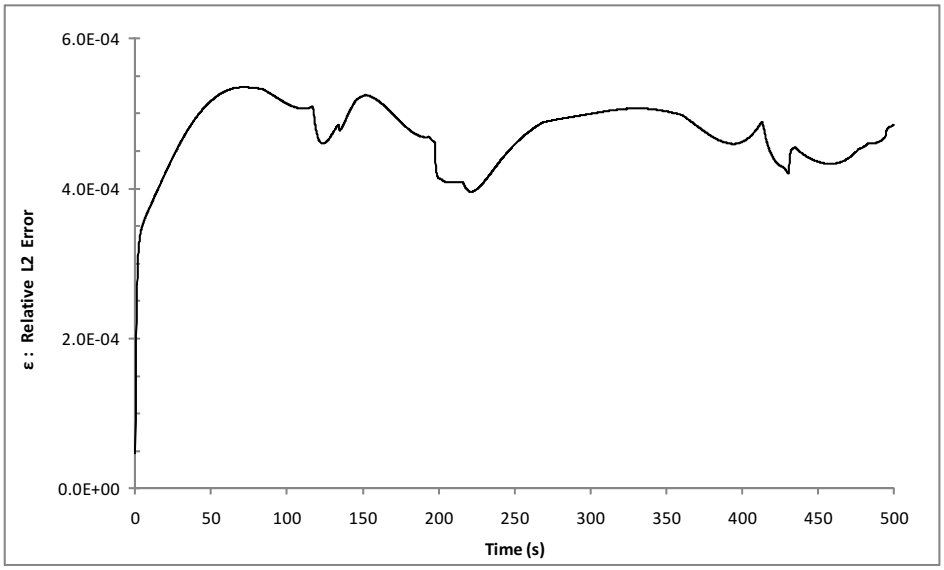

Figure 7: Variation of L_2 relative error with time: 3D test-case

The Kirchhoff transformation is applied to the thermal conductivity in order to significantly reduce the nonlinearity of the governing equation. The functions describing the variation of the required material properties with temperature can be reconstructed from pointwise experimental data using a 1D RBF interpolation procedure. These same interpolation systems can then be used to transform the material property functions to the Kirchhoff-transform variable, allowing solution of the weakly nonlinear transformed equation. The Kirchhoff transformation procedure also transforms the heat-flux boundary operator from a nonlinear operator in temperature to a linear operator in the Kirchhoff variable.

The proposed formulation is validated using two numerical examples on 3D datasets. In both cases the variation of the solution error with time is examined, and in both cases the solution is replicated to a good degree of accuracy. Each numerical example is considered in two separate configurations. The first numerical example uses a hypothetical material with a constant heat capacity and a linearly varying thermal conductivity, with a mixture of imposed temperature and imposed temperature-gradient boundary conditions. The analytical solution profile is replicated accurately even when a singularity is present on the temperature-gradient boundary of the domain, although more accurate results are obtained when the domain is translated away from the singularity.

The numerical second example uses a real-world material (zirconium), with the required material properties reconstructed from pointwise experimental data using the 1D RBF interpolation procedure. An analytical solution is imposed, via the use of suitable boundary conditions and a suitable body-source term. The LHI solution is compared against a full-domain Kansa RBF collocation method from the literature, with the two methods predicting very similar results. The LHI method, however, has the benefit of enhanced scalability to large datasets in comparison to the full-domain Kansa RBF method. As with all full-domain RBF methods, the Kansa approach will suffer from numerical ill conditioning and high computational cost as it is scaled to large datasets. A fully 3D version of the same problem

is also performed, using a different imposed analytical solution. This fully 3D problem provides more a significantly more accurate solution than with the pseudo-2D problem.

Acknowledgement:

The present work has been partially supported by the European Commission MUSTANG project (Project Reference: 227286), seventh framework program.

References

[1] S.M. Liao and T.S.Zhao. Measurements of heat transfer coefficients from supercritical carbon dioxide flowing in horizontal mini/nano channels. *Journal of Heat Transfer*, 124:413–420, 2002.

[2] J.H. Song, H.Y. Kim, H. Kim, and Y.Y. Bae. Heat transfer characteristics of a supercritical fluid flow in a vertical pipe. *Supercritical Fluids*, 44:164–171, 2008.

[3] W. R. Madych and A Nelson, S. Multivariate interpolation and conditionally positive definite functions ii. *Math. Comput.*, 54:211–230, 1990.

[4] T.A. Driscoll and B. Fornberg. Interpolation in the limit of increasingly flat radial basis functions. *Comput. Math. Appl.*, 43:413–422, 2002.

[5] Robert Schaback. Multivariate interpolation and approximation by translates of a basis function. In *Approximation Theory VIII*, 1995.

[6] D. Brown. On approximate cardinal preconditioning methods for solving pdes with radial basis functions. *Engineering Analysis with Boundary Elements*, 29:343–353, 2005.

[7] R.K. Beatson, J.B. Cherrie, and C.T. Mouat. Fast fitting of radial basis functions: Methods based on preconditioned gmres iteration. *Advances in Computational Mathematics*, 11:253–270, 1999.

[8] L. Ling and E.J. Kansa. A least-squares preconditioner for radial basis functions collocation methods. *Advances in Computational Mathematics*, 23:31–54, 2005.

[9] B.J.C. Baxter. Preconditioned conjugate gradients, radial basis functions, and Toeplitz matrices. *Comput. Math. Appl.*, 43:305–318, 2002.

[10] L. Ling and R. Schaback. On adaptive unsymmetric meshless collocation. In S.N. Atluri and A.J.B. Tadeu, editors, *Proceedings of the 2004 International Conference on Computational and Experimental Engineering and Sciences*. Tech. Science Press, Madeira, Portugal, 2004.

[11] L. Ling, R. Opfer, and R. Schaback. Results on meshless collocation techniques. *Engineering Analysis with Boundary Elements*, 30:247–253, 2006.

[12] A. Hernandez-Rosales and H. Power. Non-overlapping domain decomposition algorithm for the Hermite radial basis function meshless collocation approach: applications to convection diffusion problems. *Journal of Algorithms and Technology*, 33:127–159, 2007.

[13] X. Zhou, Y.C. Hon, and J. Li. Overlapping domain decomposition method by radial basis functions. *Appl. Numer. Math.*, 44:241–255, 2003.

[14] Yunxin Zhang. Reconstruct multiscale functions using different rbfs in different subdomains. *Appl. Math. Comput.*, 189:893–901, 2007.

[15] A.S.M. Wong, Y.C. Hon, T.S. Li, S.L.Chung, and E.J. Kansa. Multizone decomposition for simulation of time-dependent problems using the multiquadric scheme. *Comput. Math. Appl.*, 37:23–43, 1999.

[16] Z. Wu. Compactly supported positive definite radial basis functions. *Adv. Comput. Math.*, 4:75–97, 1995.

[17] H. Wendland. Piecewise polynomial, positive definite and compactly supported radial basis functions of minimal degree. *Adv. Comput. Math.*, 4:389–396, 1995.

[18] R. Schaback. On the efficiency of interpolation by radial basis functions. In A. LeMehaute, C.Rabut, and L.L.Schumaker, editors, *Surface Fitting and Multiresolution Methods*, pages 309–318. Vanderbilt University Press, Nashville, TN, 1997.

[19] G.E. Fasshauer. Solving differential equations with radial basis functions: Multilevel methods and smoothing. *Advances in Computational Mathematics*, 11:139–159, 1999.

[20] C. Lee, X. Liu, and S. Fan. Local multiquadric approximation for solving boundary value problems. *Computational Mechanics*, 30:396–409, 2003.

[21] B. Sarler and R. Vertnik. Meshless explicit local radial basis function collocation methods for diffusion problems. *Comput. Math. Appl.*, 51:1269–1282, 2006.

[22] E. Divo and A. Kassab. An efficient localised radial basis function meshless method for fluid flow and conjugate heat transfer. *Journal of Heat Transfer*, 129:124–136, 2007.

[23] G. Wright and B. Fornberg. Scattered node compact finite difference-type formulas generated from radial basis functions. *J. of Comput. Phys.*, 212:99–123, 2006.

[24] D. Stevens, H. Power, M. Lees, and H. Morvan. The use of PDE centres in the local RBF Hermitian method for 3D convective-diffusion problems. *J. Comput. Phys.*, 228:4606–4624, 2009.

[25] D. Stevens, H. Power, and H. Morvan. An order-N complexity meshless algorithm for transport-type PDEs, based on local Hermitian interpolation. *Engineering Analysis with Boundary Elements*, 33:425–441, 2009.

[26] D. Stevens, H. Power, M. Lees, and H. Morvan. A meshless solution technique for the solution of 3D unsaturated zone problems, based on local Hermitian interpolation with radial basis functions. *Transport in Porous Media*, 79:149–169, 2009.

[27] D Stevens and H Power. A scalable and implicit meshless rbf method for the 3D unsteady nonlinear Richards equation, with single and multi-zone domains. *International Journal for Numerical Methods in Engineering*, (submitted):., 2009.

[28] J.P. Holman. *Heat Transfer*. McGraw-Hill, New York, 2002.

[29] A. Bejan. *Heat Transfer*. John Wiley and Sons, New York, 1993.

[30] F. Kreith and M. Bohn. *Principles of Heat Transfer (sixth edition)*. Brooks/Cole, Pacific Grove, CA, 2000.

[31] W. Shen and S. Han. An explicit TVD scheme for hyperbolic heat conduction in complex geometry. *Numerical Heat Transfer, Part B: Fundamentals*, 41:565–590, 2002.

[32] S. Chantasiriwan. Multiquadric collocation method for time-dependent heat conduction problems with temperature-dependent thermal properties. *Journal of Heat Transfer*, 129:109–113, 2007.

[33] J. Sladek, V. Sladek, Ch. Zhang, and P. Solek. Application of the mlpg to thermo-piezoelectricity. *CMES: Computer Modeling in Engineering Sciences*, 22:217–234, 2007.

[34] Liviu Marin. The method of fundamental solutions for inverse problems associated with the steady-state heat conduction in the presence of souces. *CMES: Computer Modeling in Engineering Sciences*, 30:99–122, 2008.

[35] J. Sladek, V. Sladek, C. Tan, and S.N. Alturi. Analysis of transient heat conduction in 3d anisopropic functionally graded solids, by the mlpg method. *CMES: Computer Modeling in Engineering Sciences*, 32:161–174, 2008.

[36] G.C. Bourantas, E.D. Skouras, and G.C. Nikiforidis. Adaptive support domain implementation on the moving least squares approximation for Mfree methods applied on elliptic and parabolic PDE problems using strong-form description. *CMES: Computer Modeling in Engineering Sciences*, 43:1–25, 2009.

[37] G. Kosec and B. Sarler. Solution of phase change problems by collocation with local pressure correction. *CMES: Computer Modeling in Engineering Sciences*, 47:191–216, 2009.

[38] J. Sladek, V. Sladek, P.H. Wen, and Y.C. Hon. The inverse problem of determining heat transfer coefficients by the mesless local Petrov-Galerkin method. *CMES: Computer Modeling in Engineering Sciences*, 48:191–218, 2009.

[39] Z. Wu. Hermite-Birkhoff interpolation of scattered data by radial basis functions. *Approximation Theory and its Applications*, 8:1–11, 1992.

[40] R. Schaback. Convergence of unsymmetric kernal-based meshless collocation methods. *SIAM Journal on Numerical Analysis*, 45:333–351, 2007.

[41] R.L. Hardy. Multiquadric equations of topography and other irregular surfaces. *J. Geophys. Res.*, 176:1905–1915, 1971.

[42] E. J. Kansa. Multiquadrics - a scattered data approximation scheme with applications to computational fluid-dynamics-i: Surface approximations and partial deriviatives estimates. *Comput. Math. Appl.*, 19:127–145, 1990.

[43] E. J. Kansa. Multiquadrics - a scattered data approximation scheme with applications to computational fluid dynamics-ii: Solution to parabolic, hyperbolic and elliptic partial differential equations. *Comput. Math. Appl.*, 19:147–161, 1990.

[44] M. Zerroukat, H. Power, and C.S. Chen. A numerical method for heat transfer problems using collocation and radial basis functions. *International Journal for Numerical Methods in Engineering*, 42:1263–1278, 1998.

[45] Y.C. Hon and X.Z. Mao. An efficient numerical scheme for Burgers equation. *Appl. Math. Comput.*, 95:37–50, 1998.

[46] Y.C. Hon, K.F. Cheung, X.Z.Mao, and E.J. Kansa. A multiquadric solution for shallow water equation. *ASCE J. Hydraulic Engineering*, 125:524–533, 1999.

[47] Y.C. Hon and X.Z. Mao. A radial basis function method for solving options pricing modelling. *Financial Engineering*, 8:31–50, 1999.

[48] Y.C. Hon and R. Schaback. On unsymmetric collocation by radial basis functions. *J. Appl. Math. Comp.*, 119:177–186, 2001.

[49] G. E. Fasshauer. Solving partial differential equations by collocation with radial basis functions. In A. Le M'ehaut'e, C. Rabut, and L.L. Schumaker, editors, *Surface Fitting and Multiresolution Methods*, pages 131–138. Vanderbilt University Press, 1997.

[50] Z. Wu. Solving PDEs with radial basis functions and the error estimation. In Z. Chen, Y.Li, C.A. Micchelli, Y. Xu, and M Dekkon, editors, *Adv. in Comput. Math., Lectures in Pure and Applied Mathematics*, volume 202, 1998.

[51] A. Hernandez, A. LaRocca, and H. Power. Radial basis function Hermite collocation approach for the numerical simulation of the effect of precipitation inhibitor on the crystallization process of an oversaturated solution. *Numerical Methods for Partial Differential Equations*, 22:361–380, 2005.

[52] A. LaRocca, H.Power, V. LaRocca, and M. Morale. A meshless approach based upon radial basis function hermite collocation method for predicting the cooling and the freezing times of foods. *Computers Materials and Continua*, 2:239–250, 2005.

[53] H. Power and V. Barraco. A comparison analysis between unsymmetric and symmetric radial basis function collocation methods for the numerical solution of partial differential equations. *Comput. Math. Appl.*, 43:551–583, 2002.

[54] A. LaRocca and H. Power. A double boundary collocation Hermitian approach for the solution of steady state convection diffusion problems. *Comput. Math. Appl.*, 55:1950–1960, 2007.

[55] D. Stevens, H. Power, M. Lees, and H. Morvan. A local Hermitian RBF meshless numerical method for the solution of multi-zone problems. *Numerical Methods for Partial Differential Equations*, (submitted):–, 2009.

[56] T. Cecil, J. Qian, and S. Osher. Numerical methods for high dimensional Hamilton-Jacobi equations using radial basis functions. *J. Comput. Phys.*, 196(1):327–347, 2004.

[57] R.E. Carlson and T.A. Foley. The parameter R2 in multiquadric interpolation. *Comput. and Math. with Appl.*, 21:29–42, 1991.

[58] S. Rippa. An algorithm for selecting a good value for the parameter c in radial basis function interpolation. *Advances in Computational Mathematics*, 11:193–210, 1999.

[59] W. Rohsenow, J. Hartnett, and E. Ganic. *Handbook of Heat Transfer Fundamentals (second edition).* McGraw-Hill Book Company, New York, 1985.

[60] S. Kim. A simple direct estimation of temperature-dependent thermal conductivity with Kirchhoff transformation. *International Communications in Heat and Mass Transfer*, 28:537–544, 2001.